DOI: 10.1002/ejic.200700288

Synthesis, Structure, Electrochemistry, and Mössbauer Effect Studies of the Ferraphosphadicarbollides $[(C_5R_5)Fe(PC_2B_8H_{10})]$ (R = H, Me)

Alexander R. Kudinov,*[a] Rolfe H. Herber,*[b] Piero Zanello,*[c] Dmitry S. Perekalin,[a] Ivan V. Glukhov,[a] Israel Nowik,[b] Maddalena Corsini,[c] Serena Fedi,[c] and Franco Laschi[c]

Keywords: Iron / Carboranes / Electrochemistry / X-ray diffraction / Mössbauer spectroscopy

Reaction of the phosphadicarbollide anion $[7,8,9\text{-}PC_2B_8H_{10}]^-$ (**4**) with $[CpFe(C_6H_6)]^+$ or $[Cp^*Fe(MeCN)_3]^+$ gives the expected 12-vertex ferraphosphadicarbollides $[1\text{-}C_5R_5\text{-}1,2,3,4\text{-}FePC_2B_8H_{10}]$ [R = H (**5a**), Me (**5b**); the metal atom is assigned number 1] in around 35 % yield. Compounds **5a**,**b** undergo selective polyhedral rearrangement at 150 °C to give the corresponding isomers $[1\text{-}C_5R_5\text{-}1,2,4,5\text{-}FePC_2B_8H_{10}]$ (**6a**,**b**). The structure of **5a** has been determined by X-ray diffraction. An electrochemical investigation has revealed that all the compounds obtained display the Fe^{II}/Fe^{III} oxidation process with features of chemical reversibility on the cyclic voltammetric timescale. However, only cation $[\mathbf{6b}]^+$ is reasonably stable on the long timescales of electrolysis. Ferraphospadicarbollides **5a** and **6a** are more difficult to oxidize than the related dicarbollide and tricarbollide derivatives $[CpFe(C_2B_9H_{11})]^-$ and $[CpFe(C_3B_8H_{11})]$, respectively. Temperature-dependent Mössbauer effect studies show that the recoil-free fraction over the temperature interval 110–342 K for **5a** is well accounted for by a linear regression, and a calculation of the root-mean-square-amplitude-of-vibration (rmsav) of the iron atom, based on the Mössbauer effect (ME) data, is in reasonable agreement with the value calculated from the single-crystal X-ray study at 120 K. Similarly, the ME and X-ray rmsav data for **6a** at 293 K are in excellent agreement with each other, and the value at 120 K calculated for **6a** is in good agreement with that observed for **5a**. The metal atom motion is nearly isotropic with respect to the major symmetry axis running through the Cp ring and the Fe atom.

Introduction

The ferracarborane anion $[CpFe(C_2B_9H_{11})]^-$ ($[\mathbf{1}]^-$)[1] can be considered as a ferrocene analog, although the different charges of the $[C_2B_9H_{11}]^{2-}$ and Cp^- ligands lead to significant differences in the properties of $[\mathbf{1}]^-$ and $FeCp_2$. The use of monoanionic carborane ligands of two types, namely $[C_3B_8H_{11}]^-$ and $[9\text{-}L\text{-}7,8\text{-}C_2B_9H_{10}]^-$ (L = SMe_2, NMe_3, py), has allowed us to prepare closer analogs of ferrocene such as ferratricarbollides **2**, **3**[2] and charge-compensated ferradicarbollides $[CpFe(L\text{-}C_2B_9H_{10})]$ (for the meaning of the circles, see Scheme 1).[3]

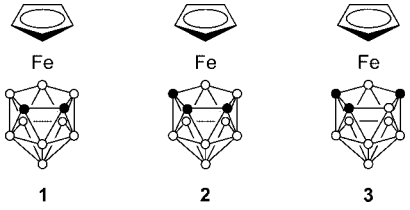

We have recently shown that combined structural, electrochemical, and Mössbauer effect (ME) studies can provide detailed information concerning the static and dynamic properties of cyclopentadienylferracarboranes and their monocations.[3a] In particular, we showed that the replacement of a boron atom by carbon results in an increase of the electron-withdrawing properties of the carborane ring. Herein we report the extension of these investigations to a number of cyclopentadienylferraphosphadicarbollides in order to elucidate the effect of a phosphorus atom on the chemical and physico-chemical characteristics of these unique compounds.

Results and Discussion

Synthesis

Štibr et al. have recently reported the synthesis of the first ferraphosphadicarbollide complex [1-Cp-1,2,3,5-

[a] A. N. Nesmeyanov Institute of Organoelement Compounds, Russian Academy of Science,
28 ul. Vavilova, 119991 Moscow, GSP-1, Russian Federation
Fax: +7-495-135-5085
E-mail: arkudinov@ineos.ac.ru
[b] Racah Institute of Physics, The Hebrew University,
91904 Jerusalem, Israel
E-mail: herber@vms.huji.ac.il
[c] Dipartimento di Chimica, Università di Siena,
Via Aldo Moro, 53100 Siena, Italy
E-mail: zanello@unisi.it
Supporting information for this article is available on the WWW under http://www.eurjic.org or from the author.

$FePC_2B_9H_{10}$] (**6a**) by interaction of 7,8,9-$PC_2B_8H_{11}$ with $[CpFe(CO)_2]_2$ in refluxing xylene.[4] However, owing to the drastic conditions, the reaction was accompanied by nonselective polyhedral rearrangements that gave a mixture of isomers.

We have found previously that room-temperature reactions of carborane anions with the $[CpFe]^+$ fragment (generated photochemically from $[CpFe(C_6H_6)]^+$) can be used for the synthesis of various ferracarboranes.[2,3,5] Employing this method with $[CpFe(C_6H_6)]^+$ and the phosphadicarbollide anion [7,8,9-$PC_2B_8H_{10}]^-$ (**4**) gave the unrearranged complex [1-Cp-1,2,3,4-$FePC_2B_9H_{10}$] (**5a**)[6] in 37% yield (Scheme 1). The pentamethylated derivative **5b** was obtained in 35% yield by reaction of **4** with the $[Cp^*Fe(MeCN)_3]^+$ cation. A significant amount (approx. 40%) of anion **4** remains unreacted in both cases, in accordance with the moderate yields, and this remains the same regardless of changes in reaction time/temperature. This may be due to σ-coordination of $[(C_5R_5)Fe]^+$ fragments to the phosphorus lone pair of anion **4**, which suppresses the formation of the π-complex.[7]

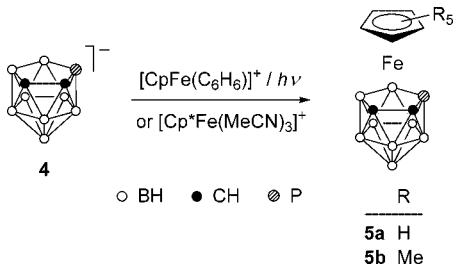

Scheme 1. Synthesis of complexes **5a**,**b**.

Complexes **5a**,**b** both undergo polyhedral rearrangement upon heating in refluxing nonane (150 °C) to give the 1,2,4,5-isomers **6a**,**b** (approx. 80% yield; Scheme 2). This rearrangement is highly selective, and no other isomers could be detected in the reaction mixture by means of ^{11}B and ^{31}P NMR spectroscopy. This observation is in sharp contrast to the nonselective isomerization of the analogous cobalt complex [1-(η^4-C_4Me_4)-1,2,3,4-$CoPC_2B_9H_{10}$] at 110 °C[5] and the nonselective further rearrangement of **6a** in refluxing mesitylene.[8] The **5a** → **6a** isomerization process is exothermic by 12.8 kcal mol^{-1}, as estimated by DFT calculations at the B3LYP/6-31G* level.[9]

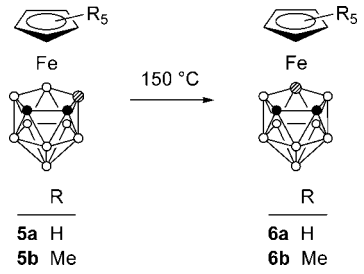

Scheme 2. Polyhedral rearrangement of complexes **5a**,**b**.

Compounds **5a**,**b** and **6a**,**b** were characterized by elemental analysis and ^1H, ^{11}B, and ^{31}P NMR spectroscopy. The ^{11}B signal assignment in **5a** and **6a** was performed with the help of DFT/GIAO calculations. The structure of **5a** was also investigated by X-ray diffraction (Figure 1).[10] The carbon atoms of the Cp ring as well as the P1 and B5 atoms were found to be disordered over two positions. The C3–C4 distance (1.609 Å) is notably longer than a typical C–C single bond but is in the usual range for *closo*-metallacarboranes.[11] The average Fe–C_{cage} (2.020 Å) and Fe–P (2.237 Å) distances are close to those for isomer **6a** (2.018 and 2.251 Å).[4] The Fe···Cp distance in **5a** (1.683 Å) is also close to that in **6a** (1.681 Å), thus indicating similar coordinating properties of the isomeric phosphadicarbollide anions [7,8,9-$PC_2B_8H_{10}]^-$ and [7,9,10-$PC_2B_8H_{10}]^-$. The significantly longer Fe···Cp distances in **5a** and **6a** than in $FeCp_2$ (1.660 Å)[12] suggest a greater acceptor ability of the phosphadicarbollide ligands relative to Cp^-, in accordance with the electrochemical data (see below).

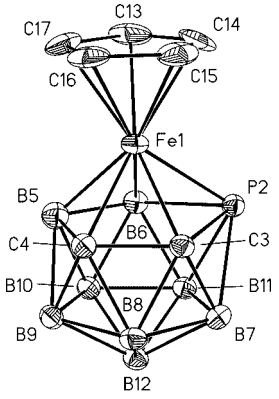

Figure 1. The molecular structure of **5a** (thermal ellipsoids at 50% probability). The hydrogen atoms and the second conformation of the Cp ring have been omitted for clarity. Selected interatomic distances [Å]: Fe1–P2 2.231(2), Fe1–C3 2.017(2), Fe1–C4 2.023(2), Fe1–B5 2.062(6), Fe1–B6 2.172(4), Fe1–C13 2.065(5), Fe1–C14 2.046(7), Fe1–C15 2.077(4), Fe1–C16 2.084(4), Fe1–C17 2.071(4), P2–B6 2.008(3), P2–C3 2.033(3), C3–C4 1.609(3).

Mössbauer Effect (ME) Studies

As noted previously,[13] all diamagnetic iron compounds in which the sole metal atom does not occupy a cubic symmetry site give rise to doublet ME spectra which are characterized by their isomer shift (IS) and quadrupole splitting (QS) parameters. A typical ME spectrum (that of **6a** at 90 K) is shown in the bottom trace of Figure 2.

The ME parameters for compound **5a** are summarized in Table 1. The data for the Fe^{III} complex [1-Cp-1,2,3-$FeC_2B_9H_{11}$] (**1**) are also included for comparison purposes. The temperature dependence of the IS of **5a** is well fitted by a linear regression in the range 110–342 K (correlation coefficient for 12 data points: 0.997) from which the effective vibrating mass M_{eff} is calculated to be 94 ± 1 Da.[14] The difference between this value and the "bare" iron atom mass of 57 Da reflects the covalency of the metal–ligand

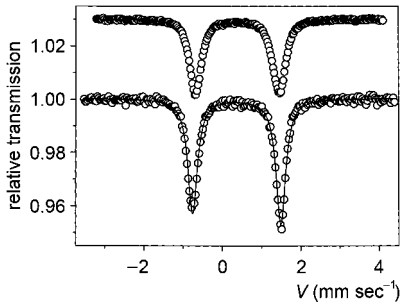

Figure 2. Mössbauer spectra of **6a** (bottom trace) and **6b** (top trace) at 90 K. The presence of a single Fe site is evident from the figure. The velocity scale is with reference to the centroid of an α-Fe absorber spectrum at room temperature.

interaction. It is worth noting that the IS of **5a** is significantly smaller than that of ferrocene itself (0.536 ± 1 mm s^{-1} at 90 K) and is slightly larger than that of **1** under the same conditions. The latter increase implies a decrease in the electron density at the metal atom center (since $\Delta r^2/r^2$ is negative for ^{57}Fe), presumably due to an increase of the acceptor character of the ligand upon replacement of a B atom by P. The temperature dependence of the recoil-free fraction, extracted from the temperature dependence of ln A (where A is the area under the resonance curve for an optically thin absorber), is shown graphically in Figure 3 and is again well fitted by a linear regression.

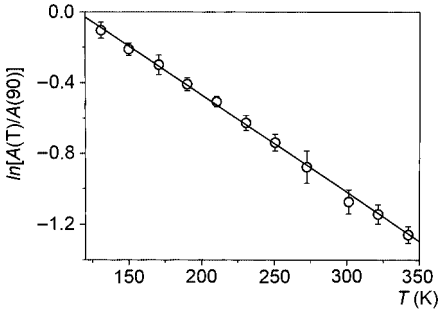

Figure 3. Temperature-dependence of the normalized logarithm of the area under the resonance curve for **5a**. The slope is $-(5.50 \pm 0.07) \times 10^{-3}$ K^{-1} and the correlation coefficient for the 11 data points is 0.999.

As has been noted previously,[15] the recoil-free fraction data can be directly related to the U_{ij} values for the iron atom determined from a single-crystal X-ray diffraction study. The average U_{ij} value for **5a** at 120(2) K is 0.01740 Å^2. This translates into a root-mean-square-amplitude-of-vibration (rmsav) of the iron atom of 0.132 Å. The corresponding value extracted from the ME recoil-free fraction data is 0.111 Å, which is only a modest agreement. The analogous value for the dicarbollide complex **1** is $<x^2>^{1/2}_{ME} = 0.145$ Å, while $<x^2>^{1/2}_{X}$ is 0.151 Å at 120 K. The introduction of a P atom into the five-membered carborane face clearly leads to a small shortening of the rmsav of Fe. The area ratio, $R = [A(+)/A(-)]$ (where + and – indicate the position on the velocity scale of the resonance line with respect to the spectrum centroid), of the two QS components of the ME spectra shows only a very small temperature dependence, thereby indicating that the iron atom motion is nearly isotropic over the temperature range 91–341 K.

The ME spectroscopic results for **6a** are very similar to those observed for **5a** (see Table 1). Two points, however, must be made. First of all, the area ratio R shows a significantly larger temperature dependence, which implies a larger anisotropy in the metal atom motion in **6a** compared to **5a** as a result of having the ring P atom flanked by two BH groups rather than flanked by a BH and a CH group as in **5a**. Secondly, the average U_{ij} value reported for iron in the crystal structure of **6a** determined at 293(2) K[4] is 0.0344 Å^2, which translates into an rmsav of the iron atom of 0.183 Å. From the temperature dependence of the area under the resonance curve in the interval 135–303 K, the corresponding rmsav of the iron atom at 293 K is 0.180 Å, which is in good agreement (within 3.1%) with the X-ray value. Moreover, the rmsav value calculated from the ME data obtained at 120 K is 0.115 Å, which is in excellent agreement with the corresponding data reported for **5a** (see above) at the same temperature.

The ME spectroscopic parameters for the methylated compounds **5b** and **6b** are also given in Table 1. It should be noted that, while the IS parameters at 90 K are not sensitive to the replacement of Cp by Cp*, the QS parameters show a decrease of almost 0.123 ± 0.009 mm s^{-1}. Qualitatively, it may be surmised that the presence of the methyl groups increases the metal atom–ring distance and hence leads to a decrease in the electric field gradient at the metal center (see below). However, this increase is not sensitively reflected in the relative IS values as referred to above. The temperature dependence of ln[$A(T)$/A(90)] for both compounds is well accounted for by a linear regression. It should be noted, however, that the data for **6b** could only be extended over the range 90–272 K. At 272 K, the resonance

Table 1. Mössbauer parameters for the compounds discussed in the text.

	5a	**6a**	**5b**	**6b**	**1**[a]
IS(90) [mm s^{-1}]	0.384(4)	0.370(1)	0.358(5)	0.374(6)	0.337(3)
QS(90) [mm s^{-1}]	2.147(4)	2.248(1)	2.069(5)	2.082(6)	0.525(3)
–d(IS)/d(T) [10^{-4} mm s^{-1} K^{-1}]	4.43(3)[b]	5.12(22)[c]	4.54(27)[d]	4.27(14)[e]	5.3(3)
–d(lnA)/d(T) [10^{-3} K^{-1}]	5.50(7)[f]	5.88(9)[g]	6.90(28)[h]	7.47(9)[i]	7.9(1)
M_{eff} [Da]	94 ± 1	81 ± 3	92 ± 5	97 ± 3	78(4)
Θ_M [K]	123	127	111	103	113

[a] Data taken from ref.[3a] [b] Ranges for determining "high temperature" slopes (see text): 110–342 K. [c] 150–342 K. [d] 150–322 K. [e] 170–272 K. [f] 110–342 K. [g] 130–302 K. [h] 90–320 K. [i] 111–272 K.

effect magnitude was found to be only around 1.3% and more than 6.6 million counts per channel were acquired to provide the necessary statistical accuracy.

Unfortunately, due to excessive crystalline disorder, it has not proved possible to acquire meaningful single X-ray data for these two compounds. However, it is possible to extract rmsav data for the iron atom at 120 K by assuming that the Mössbauer recoil-free fraction data are reasonably reliable over the cited temperature range. These vibrational amplitudes are 0.125 and 0.130 Å for **5b** and **6b**, respectively, and suggest an increase of this amplitude by about 0.014 Å on replacing Cp by Cp*, which agrees with the QS parameter results cited above. A comparison of the temperature dependence of $\ln[A(T)/A(90)]$ for **5a**, **5b**, and **1** is summarized in Figure 4.

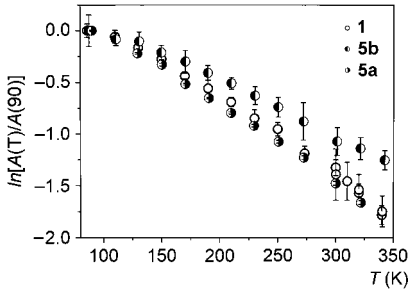

Figure 4. Temperature dependence of $\ln[A(T)/A(90)]$ for **5a** and **5b** showing the effect of substitution in the cyclopentadienido ring on the recoil-free fraction.

The slope difference between **5a** and **5b** provides evidence for lattice "softening" due to this interchange but is unexpected in view of the presumed increase in the metal atom–ring distance due to the presence of the methyl groups in the ring. A possible explanation for this observation lies in the assumption that replacing Cp with Cp* results in the presence of one or more low frequency vibrational modes that affect the dynamics of the whole molecule rather than just the metal atom center. In other words, both intra- and intermolecular motions must be considered to explain this observation. Note, however, that the Mössbauer lattice temperature,[15] Θ_M, is smaller for **5b** and **6b** than for **5a** and **6a**.

Finally, it is worth noting that neither **5b** nor **6b** show a significant temperature dependence on R. The average value of this parameter for **5b** is 1.04 ± 0.01 over the range 90–322 K, which indicates an essentially isotropic motion of the metal atom parallel and perpendicular to the principal symmetry axis running through the metal atom.

Electrochemistry

Figure 5 gives an overall picture of the Fe^{II}/Fe^{III} electron-transfer process in the ferraphosphacarboranes **5a**,**b** and **6a**,**b**. The formal electrode potentials of the redox processes studied are compiled in Table 2, together with that of the classical dicarbollide [1-Cp-1,2,3-$FeC_2B_9H_{11}$] (**1**) and the ferratricarbollide isomers [1-Cp-1,2,3,4-$FeC_3B_8H_{11}$] (**2**) and [1-Cp-1,2,3,5-$FeC_3B_8H_{11}$] (**3**).

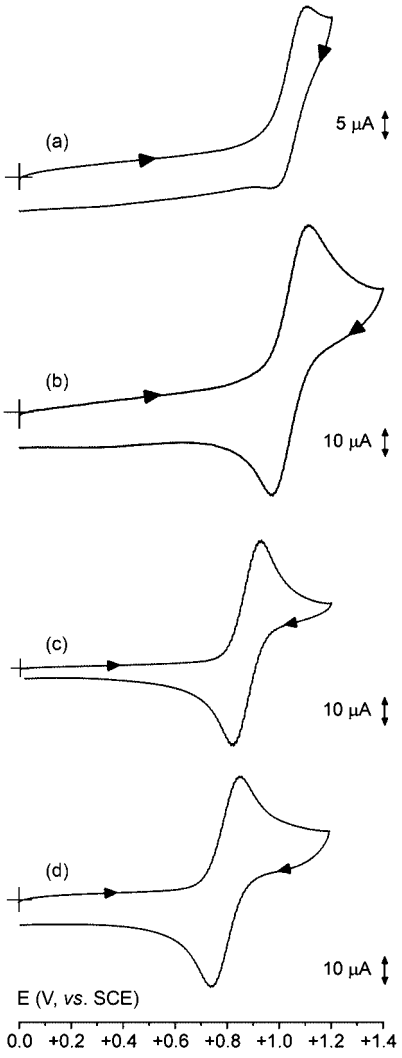

Figure 5. Comparison of the cyclic voltammetric responses given by ferraphosphacarboranes **5a**,**b** and **6a**,**b**: (a) **5a** (0.7×10^{-3} M); (b) **6a** (1.2×10^{-3} M); (c) **5b** (1.0×10^{-3} M); (d) **6b** (0.7×10^{-3} M). CH_2Cl_2 solutions contain $[Bu_4N][PF_6]$ (0.2 M) as supporting electrolyte. Gold working electrode. Scan rate: 0.5 $V s^{-1}$.

Table 2. Formal electrode potentials (V vs. SCE), peak-to-peak separation (mV), and current ratio for the redox changes exhibited by the compounds in CH_2Cl_2 solution.

Compound	$E^{\circ\prime}_{Fe(II)/Fe(III)}$	ΔE_p[a]	i_{pc}/i_{pa}[b]	$E^{\circ\prime}_{Fe(II)/Fe(I)}$[a]
5a	+1.05	94[b]	0.3	–1.67[c]
6a	+1.05	104[b]	0.7	–1.85[c]
5b	+0.88	65	0.9	–1.78[c]
6b	+0.79	74	1.0	[d]
1[e]	–0.18	84	1.0	–
2[e]	+0.74	72	0.8	[d]
3[e]	+0.82	73	1.0	[d]

[a] Measured at 0.1 $V s^{-1}$. [b] Measured at 0.5 $V s^{-1}$. [c] Peak potential for irreversible processes. [d] Overlapped by the solvent discharge. [e] Data taken from ref.[3a]

The position of the phosphorus atom in the coordinating PC_2B_2 pentagonal face for the non-methylated compounds **5a** and **6a** seems to affect the kinetic rather than the thermodynamic parameters of the pertinent oxidation pro-

cesses. In fact, while both processes occur at the same formal electrode potential (see Table 2), there is a marked difference in the chemical stability of monocations $[\mathbf{5a}]^+$ and $[\mathbf{6a}]^+$, as measured by the current ratio i_{pc}/i_{pa}, which is equal to 0.4 s for **5a** and 0.9 s for **6a** at 2.0 $V s^{-1}$. As a consequence, assuming that a first-order chemical reaction accompanies the Fe^{II}/Fe^{III} change, a lifetime of 0.2 and 6 s can be calculated for $[\mathbf{5a}]^+$ and $[\mathbf{6a}]^+$, respectively.

The opposite trend holds for the methylated derivatives **5b** and **6b**: their monocations seem to be stable on the cyclic voltammetric time scale (i_{pc}/i_{pa} almost constantly equal to 1 with an increase of the scan rate), although their formal electrode potentials are somewhat different (see Table 2). In reality, the electrogenerated monocation $[\mathbf{5b}]^+$ proved to be unstable under exhaustive macroelectrolysis at room temperature (20 °C), whereas $[\mathbf{6b}]^+$ is reasonably stable (a minor trace of an unidentified species able to oxidize reversibly at $E°' = +1.1$ V appeared). Thus, the original pink-orange solution of **6b** (λ_{max} = 482 nm) turns pale green upon exhaustive one-electron oxidation and displays a new band at 780 nm with a shoulder at 650 nm.

It should be also noted that all the ferraphosphacarboranes display an essentially irreversible Fe^{II}/Fe^{I} reduction.

As previously pointed out,[3a] the replacement of a boron atom by a carbon atom in the coordinating pentagon of the dicarbollide ligand (i.e. passing from **1** to the isomeric species **2** and **3**) makes the Fe^{II}/Fe^{III} oxidation dramatically more difficult (by about 1 V). We now find that the replacement of a carbon atom in the ferratricarbollides for a phosphorus atom (i.e. passing from **2** and **3** to **5a** and **6a**, respectively) further increases the oxidation potentials (by about 0.3 V). Unfortunately, we have not yet been able to find an unequivocal thermodynamic effect for the non-methylated complexes resulting from the position of the phosphorus atom in the cage, although it appears that the non-adjacent position in both series increases the kinetic stability of the monocations more than the adjacent position, with the PC_2B_2 assembly lowering it more severely than C_3B_2. Obviously, the Fe^{II}/Fe^{I} reduction becomes more facile (in the order $PC_2B_2 > C_3B_2 > C_2B_3$) as a consequence of the shifts of the Fe^{II}/Fe^{III} redox potential.

In light of the complete, or almost complete, chemical reversibility of cations $[\mathbf{6a}]^+$, $[\mathbf{5b}]^+$, and $[\mathbf{6b}]^+$ at room temperature, they were electrogenerated at 253 K and characterized by EPR spectroscopy. Figure 6 shows the first-derivative X-band EPR spectrum of a CH_2Cl_2 solution of $[\mathbf{6b}]^+$ at 105 K.

The line-shape analysis was performed by assuming a low-spin Fe^{III} complex with a doublet state electron spin Hamiltonian in a strongly axial structure (Zeeman interaction).[16] The intense anisotropic signal displays two well separated [$\delta g_i = g_{\parallel} - g_{\perp}$ = 231(5) G] and unresolved absorptions (multiple derivative analysis). The g_i values ($g_{\parallel} > g_{\perp} \neq g_{electron} = 2.0023$) are typical of metallic absorptions arising from effective $3d^5$ spin-orbit λ (S = 1/2) coupling.[16] No direct ^{57}Fe hyperfine ($I_{^{57}Fe}$ = 1/2, natural abundance = 2.2%) or ^{31}P, ^{11}B, ^{10}B, ^{1}H, or ^{13}C superhyperfine ($I_{^{31}P}$ = 1/2, natural abundance = 100%; $I_{^{11}B}$ = 1/2, natural abundance = 81.2%; $I_{^{10}B}$ = 3/2, natural abundance 18.8%; $I_{^{1}H}$ = 1/2, natural abundance = 99.99%; $I_{^{13}C}$ = 1/2, natural abundance = 1.1%) splitting is evident in the two spectral regions. The computed[17] anisotropic features are collected in Table 3.

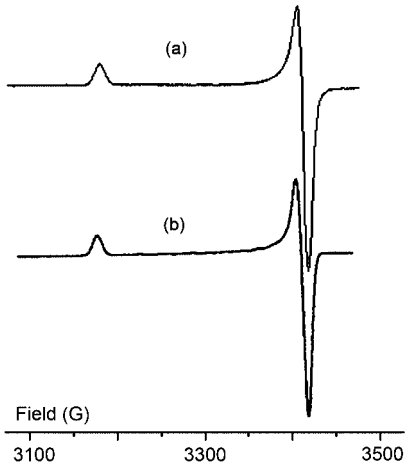

Figure 6. Experimental (a) and simulated (b) X-band EPR spectra of $[\mathbf{6b}]^+$ in CH_2Cl_2 solution containing $[Bu_4N][PF_6]$ (0.2 M). T = 105 K. ν_o = 9.68 GHz.

Table 3. EPR parameters for the electrogenerated cations $[\mathbf{5b}]^+$, $[\mathbf{6a}]^+$, and $[\mathbf{6b}]^+$ in CH_2Cl_2 solution[a] [$<g> = 1/3(g_l + g_m + g_h) = 1/3(g_{\parallel} + 2g_{\perp})$; $\delta g_{l-h} = g_l - g_h$; error in g_i and δg_{l-h}: ±0.005; error in ΔH_{iso}: ±4 G].

Complex	g_l	g_m	g_h	δg_{l-h}	$<g>$	g_{iso}[b]	ΔH_{iso}[b]
$[\mathbf{5b}]^+$	2.150	2.032	2.016	0.134	2.066	2.064	14
$[\mathbf{6a}]^+$	2.183	2.029	2.029	0.154	2.080	2.066	10
$[\mathbf{6b}]^+$	2.175	2.027	2.027	0.148	2.076	–	–

[a] T = 105 K. [b] T = 298 K.

Given the very low natural abundance of the magnetically active atoms present in the complex, particularly ^{57}Fe and ^{13}C, the spectral features are expected to be significantly obscured by the experimental anisotropic linewidths [$\Delta H_{i(exp)}$]. The paramagnetic analysis strongly indicates that the actual SOMO is mainly constituted by the 3d atomic orbitals of the Fe^{III} center, with minor contributions from the directly coordinating donor atoms.

Because of the effective speeding up of the electron paramagnetic relaxation mechanisms, raising the temperature to the glass/fluid transition causes the axial signals to disappear and the fluid solution becomes EPR-silent. Rapid refreezing restores the original anisotropic features. Such a temperature-dependent paramagnetic behavior is not unusual and is due to the effective speeding up of the electron paramagnetic relaxation mechanisms under fast motion conditions in the presence of active thermal effects.[16]

A substantially similar magnetic behavior is exhibited by the related non-methylated cation $[\mathbf{6a}]^+$, although the fluid solution (T = 298 K) exhibits a broad signal with low intensity, the g_{iso} value of which is slightly smaller than the $<g>$ value under glassy conditions because of the effective averaging of the original anisotropy.

Cation $[\mathbf{5b}]^+$ exhibits a different line-shape with a broader and unresolved rhombic pattern ($g_i \neq g_{electron}$) and a high field absorption that is partially split and overlapped. No hyperfine or superhyperfine resolution was visible in this case. In addition, a broad isotropic signal appears in the fluid solution at a g_{iso} value that is essentially identical to the $<g>$ value in glassy solution. It should be noted that the paramagnetic features (see Table 3) suggest a slightly lower metallic character of the unpaired electron.

Since the EPR spectral symmetry (isotropic, axial, rhombic) reflects the local symmetry around the paramagnetic center, in other words the structure of the SOMO, the EPR evidence for different anisotropic line-shapes and linewidths must arise from significant differences in the geometrical coordinating frameworks.[16] In the present case, the fact that cation $[\mathbf{5b}]^+$ exhibits a less symmetrical ligand framework than cations $[\mathbf{6a}]^+$ and $[\mathbf{6b}]^+$ due to the adjacent vs. nonadjacent position of the heteroatoms could be responsible for the different spectral patterns.

We carried out a multiple derivatives analysis of the best-fit experimental anisotropic line-widths (ΔH_i) in order to determine the upper limit for the unpaired electron couplings of cations $[\mathbf{5b}]^+$, $[\mathbf{6a}]^+$, and $[\mathbf{6b}]^+$ with the different magnetically active nuclei of the coordinating atoms (see Table S1 in the Supporting Information). This study clearly showed the metallic character of the X-band experimental spectra, although a significant interaction of the phosphorus nucleus seems to be involved in the magnetic interaction with the unpaired electron.

Conclusions

Reaction of the phosphadicarbollide anion **4** with $[(C_5R_5)Fe]^+$ fragments under mild conditions leads to the non-rearranged ferraphosphacarboranes **5a**,**b**, whose thermal isomerization into **6a**,**b** correlates with an increase of the thermodynamic stability, as estimated by DFT calculations. The electrochemical data for these compounds suggest a greater acceptor character of the phosphadicarbollide ligands compared with their di- and tricarbollide analogues.

The isomer shifts of **5a**,**b** and **6a**,**b** at 90 K are significantly smaller than those for ferrocenes Cp_2Fe and Cp^*_2Fe (0.536 and 0.492 mm s^{-1}, respectively, at 90 K), which reflects a higher electron density at the metal atom in the former. This observation was somewhat unexpected, since the electrochemical data and electronegativity considerations would suggest the opposite. The quadrupole splitting parameter is not sensitive to the location (adjacent or not) of the two boron atoms facing the metal center in the carbollide structure. Temperature-dependent ME measurements of the rmsav of the metal atom in **6a** are in good agreement with the value extracted from single-crystal X-ray data at 293 K.

Experimental Section

General Remarks: All reactions were carried out under argon in anhydrous solvents, which were purified and dried according to standard procedures. All products were isolated in air. The ^{1}H, ^{11}B, and ^{31}P NMR spectra were recorded with a Bruker AMX-400 instrument at room temperature in $CDCl_3$. The salt $[Bu_4N][7,8,9\text{-}PC_2B_8H_{10}]$ ($[Bu_4N][\mathbf{4}]$) was prepared by mixing $7,8,9\text{-}PC_2B_8H_{11}$[18] and Bu_4NBr in aqueous NaOH. Materials and apparatus for electrochemistry and joint EPR spectroscopy have been described elsewhere.[19] All the potential values are referred to the saturated calomel electrode (SCE). The one-electron oxidation of ferrocene occurs at $E^{\circ\prime}$ = +0.39 V under the present experimental conditions.

[1-Cp-1,2,3,4-FePC$_2$B$_8$H$_{10}$] (5a): A mixture of $[Bu_4N][\mathbf{4}]$ (230 mg, 0.6 mmol) and $[CpFe(C_6H_6)]PF_6$ (413 mg, 1.2 mmol) in CH_2Cl_2 (15 mL) was irradiated whilst stirring at room temperature for 4 h, during which time its color changed from yellow to bright-red. The reaction mixture was concentrated in vacuo and the residue eluted through a short (5 cm) silica gel column with a CH_2Cl_2/petroleum ether mixture (1:2) as eluent. Concentration of the red fraction by passing an argon stream over the solution gave red crystals of **5a** suitable for X-ray diffraction (60 mg, 37%). ^{1}H NMR: δ = 5.03 (s, 5 H, Cp), 3.88 (s, 1 H, cage-CH), 3.55 (d, $J_{^{31}P,^1H}$ = 16 Hz, 1 H, cage-CH) ppm. ^{11}B{^{1}H} NMR (exp./calcd.): δ = 1.9/3.1 (s, 1 B, B5), 0.3/–2.8 (s, 1 B, B12), –6.2/–5.0 (s, 1 B, B6), –6.4/–7.8 (s, 1 B, B10), –9.0/–10.3 (s, 1 B, B9 or B11), –10.8/–10.3 (s, 1 B, B9 or B11), –19.9/–21.4 (s, 1 B, B8), –27.0/–28.4 (s, 1 B, B7) ppm. ^{31}P NMR: δ = 27.4 (s, 1 P, P2) ppm. $C_7H_{15}B_8FeP$ (272.50): calcd. C 30.87, H 5.51, B 31.75; found C 31.07, H 5.68, B 31.40.

[1-Cp*-1,2,3,4-FePC$_2$B$_8$H$_{10}$] (5b): A mixture of $[Bu_4N][\mathbf{4}]$ (157 mg, 0.4 mmol) and $[Cp^*Fe(MeCN)_3]PF_6$ (188 mg, 0.4 mmol) in thf (10 mL) was stirred at room temperature overnight, which resulted in a color change from dark- to bright-red. The reaction mixture was concentrated in vacuo and the residue eluted through a short (5 cm) silica gel column with a CH_2Cl_2/petroleum ether mixture (1:2) as eluent. Concentration of the red fraction gave red crystals of **5b** (47 mg, 35%). ^{1}H NMR: δ = 2.88 (s, 1 H, cage-CH), 2.54 (d, $J_{^{31}P,^1H}$ = 13 Hz, 1 H, cage-CH), 1.84 (s, 15 H, Cp*) ppm. ^{11}B{^{1}H} NMR: δ = 3.0 (s, 1 B), –3.3 (s, 1 B), –4.2 (s, 1 B), –8.9 (s, 1 B), –10.5 (s, 1 B), –11.9 (s, 1 B), –20.6 (s, 1 B), –28.5 (s, 1 B) ppm. ^{31}P NMR: δ = 38.3 (s, 1 P, P2) ppm. $C_{12}H_{25}B_8FeP$ (342.63): calcd. C 42.07, H 7.35, B 25.24; found C 42.23, H 7.14, B 25.11.

Thermal Isomerization of 5a,b: Complex **5a** (100 mg) was refluxed in nonane (5 mL) for 6 h. The course of isomerization was checked every 2 h by recording the ^{11}B and ^{31}P NMR spectra. After the reaction was complete, the solution was slowly cooled to 0 °C to give bright red crystals of **6a**, which were washed with cold pentane and dried in vacuo (77 mg, 77%). Complex **6b** was obtained from **5b** in a similar manner in 83% yield. **6a:** ^{1}H NMR: δ = 4.96 (s, 5 H, Cp), 4.37 (s, 2 H, cage-CH) ppm. ^{11}B{^{1}H} NMR (exp/calc): δ = –2.1/–6.0 (s, 1 B, B12), –11.4/–11.0 (s, $J_{^{31}P,^{11}B}$ = 39 Hz, 2 B, B3,6), –13.1/–14.7 (s, 1 B, B9), –13.8/–13.1 (s, 2 B, B7,11), –21.1/–18.8 (s, 2 B, B8,10) ppm. ^{31}P NMR: δ = –14.8 (s, 1 P, P2) ppm. **6b:** ^{1}H NMR: δ = 3.40 (s, 2 H, cage-CH), 1.85 (s, 15 H, Cp*) ppm. ^{11}B{^{1}H} NMR: δ = –5.0 (s, 1 B), –9.5 (s, $J_{^{31}P,^{11}B}$ = 38 Hz, 2 B), –13.6 (s, 1 B), –14.9 (s, 2 B), –19.6 (s, 2 B) ppm. ^{31}P NMR: δ = –6.6 (s, 1 P, P2) ppm. $C_{12}H_{25}B_8FeP$ (342.63): calcd. C 42.07, H 7.35, B 25.24; found C 42.38, H 7.01, B 25.20.

Mössbauer Spectroscopy: The samples were transferred into plastic holders and mounted in a variable-temperature cryostat as described previously.[13] The methods for spectrometer calibration, data analysis, and temperature control monitoring have been detailed previously.[13] All isomer shifts (IS) are given with respect to a room-temperature α-Fe absorber spectrum which was also used for spectrometer calibration. The ME spectral line widths for the optically "thin" samples was 0.248 ± 0.013 mm s^{-1}.

X-ray Crystallography for 5a: $C_7H_{15}B_8FeP$, M = 272.49, monoclinic, space group $P2_1/c$, 120 K, a = 6.8292(12), b = 9.811(2), c = 18.015(3) Å, β = 90.816(8)°, V = 1206.9(4) Å^3, Z = 4, $F(000)$ = 552, $d_{calcd.}$ = 1.500 g cm^{-3}, μ = 1.340 mm^{-1}. The unit cell parameters and intensities of 10973 reflections were measured with a Bruker SMART 1000 CCD area detector, using graphite-monochromated Mo-K_α radiation, ϕ- and ω-scans, θ_{max} = 27°. The temperature of the crystal was maintained with a Cryostream (Oxford Cryosystems) open-flow nitrogen gas cryostat. Reflection intensities were integrated using SAINT software,[20] and absorption correction was applied semi-empirically using the SADABS program. The structure was solved by direct methods and refined by full-matrix least squares against F^2 in an anisotropic approximation for all non-hydrogen atoms except B5 and P2, which were found to be disordered over two sites with respect to the mirror plane passing through the center of the C3–C4 bond (3:2 occupancy), and the carbon atoms of the Cp ring, which were found to be disordered over two sites (4:1 occupancy). The disordered atoms were refined in an isotropic approximation. The polyhedron hydrogen atoms were located from the Fourier density synthesis and refined in an isotropic approximation. All calculations were performed using the SHELXTL software.[21] Final R factors are equal to R_1 = 0.0349 for 2068 reflections with $I > 2\sigma(I)$ and wR_2 = 0.0834 for all 2585 independent reflections. CCDC-635642 contain the supplementary crystallographic data for this paper. These data can be obtained free of charge from The Cambridge Crystallographic Data Center via www.ccdc.cam.ac.uk/data_request/cif.

Computational Details: All calculations were performed using the Gaussian 98 (revision A.7) software[22] package at the B3LYP/6-31G* level. The structures of isomers **5a** and **6a** were optimized within C_1 and C_s symmetry, respectively. The frequency calculations were performed to confirm the global minimum and include ZPE corrections to the energy. The ^{11}B NMR shifts were calculated using the GIAO method by subtracting the calculated isotropic shielding values from that of B_2H_6 (93.50 at B3LYP/6-31G*). The experimental chemical shift of B_2H_6 was assigned to be δ = 16.6 ppm.[23]

Supporting Information (see footnote on the first page of this article): Computed upper limit values of the temperature-dependent hyperfine and superhyperfine couplings of cations **[5b]**$^+$, **[6a]**$^+$, and **[6b]**$^+$ in CH_2Cl_2 solution. Details of the DFT calculations of **5a** and **6a**, including the optimized coordinates, NBO charges, and NMR shielding tensors.

Acknowledgments

This work was supported by the Division of Chemistry and Material Sciences of the Russian Academy of Sciences. P. Z. gratefully acknowledges the financial support of the University of Siena (PAR 2005).

[1] M. F. Hawthorne, R. L. Pilling, *J. Am. Chem. Soc.* **1965**, *87*, 3987–3988.
[2] D. S. Perekalin, J. Holub, D. G. Golovanov, K. A. Lyssenko, P. V. Petrovskii, B. Štíbr, A. R. Kudinov, *Organometallics* **2005**, *24*, 4387–4392.
[3] a) R. H. Herber, A. R. Kudinov, P. Zanello, I. Nowik, D. S. Perekalin, V. I. Meshcheryakov, K. A. Lyssenko, M. Corsini, S. Fedi, *Eur. J. Inorg. Chem.* **2006**, 1786–1795; b) A. R. Kudinov, V. I. Meshcheryakov, P. V. Petrovskii, M. I. Rybinskaya, *Izv. Akad. Nauk*, *Ser. Khim.* **1999**, 177–179; *Russ. Chem. Bull.* **1999**, *48*, 176–177.
[4] B. Štíbr, J. Holub, M. Bakardjiev, I. Pavlík, O. L. Tok, I. Císařova, B. Wrackmeyer, M. Herberhold, *Chem. Eur. J.* **2003**, 2239–2244.
[5] a) D. S. Perekalin, I. V. Glukhov, B. Štíbr, A. R. Kudinov, *Inorg. Chim. Acta* **2006**, *359*, 3264–3268; b) J. Holub, B. Grüner, D. S. Perekalin, D. G. Golovanov, K. A. Lyssenko, P. V. Petrovskii, A. R. Kudinov, B. Štíbr, *Inorg. Chem.* **2005**, *44*, 1655–1659.
[6] We use the numbering system in which the metal vertex bears number 1.
[7] A similar behavior has been observed for the reaction of the cation $[(C_4Me_4)Co(MeCN)_3]^+$ with $[9\text{-Cl-}7,8,11\text{-}PC_2B_8H_9]^-$, where formation of the σ-complex was confirmed by ^{31}P and ^{11}B NMR spectroscopy: E. V. Mutseneck, D. S. Perekalin, J. Holub, Z. A. Starikova, K. A. Lyssenko, P. V. Petrovskii, P. Zanello, M. Corsini, B. Štíbr, A. R. Kudinov, *Organometallics* **2006**, *25*, 2419–2426.
[8] B. Štíbr, J. Holub, M. Bakardjiev, I. Pavlík, O. L. Tok, B. Wrackmeyer, *Eur. J. Inorg. Chem.* **2003**, 2524–2528.
[9] This correlates with an energy difference of 12.2 kcal mol^{-1} calculated at the B3LYP/6-311+G**//B3LYP/6-31G* level: F. A. Kiani, M. Hofmann, *Organometallics* **2006**, *25*, 485–490.
[10] Unfortunately, the X-ray structures of **5b** and **6b** were not solved because of severe disorder and libration even at 120 K.
[11] J. M. Oliva, N. L. Allan, P. v. R. Schleyer, C. Viñas, F. Teixidor, *J. Am. Chem. Soc.* **2005**, *127*, 13538–13547.
[12] A. Haaland, J. E. Nilsson, *Acta Chem. Scand.* **1968**, *23*, 2653–2656.
[13] G. Laus, H. Schottenberger, K. Wurst, R. H. Herber, U. Griesser, *J. Phys. Chem. B* **2004**, *108*, 5082–5087.
[14] R. H. Herber, in *Chemical Mössbauer Spectroscopy* (Ed.: R. H. Herber), Plenum Press, New York, **1984**.
[15] R. H. Herber, I. Nowik, V. Kahlenberg, H. Kopacka, H. Schottenberger, *Eur. J. Inorg. Chem.* **2006**, 3255–3260, and references cited therein.
[16] a) F. E. Mabbs, D. Collison, *Electron Paramagnetic Resonance of d Transition Metal Compounds*, in *Studies in Inorganic Chemistry*, Elsevier, New York, **1992**, vol. 16; b) J. R. Pilbrow, *Transition Ion Electron Paramagnetic Resonance*, Oxford Science Publications, Oxford, **1990**; c) R. S. Drago, *Physical Methods for Chemists*, Saunders College Publ., New York; **1992**.
[17] G. P. Lozos, B. M. Hoffman, C. G. Franz, *Quantum Chemistry Program Exchange* **1974**, *11*, 265.
[18] B. Štíbr, J. Holub, M. Bakardjiev, D. Hnyk, O. L. Tok, W. Milius, B. Wrackmeyer, *Eur. J. Inorg. Chem.* **2002**, 2320–2326.
[19] P. Zanello, F. Laschi, M. Fontani, C. Mealli, A. Ienco, K. Tang, X. Jin, L. Li, *J. Chem. Soc. Dalton Trans.* **1999**, 965–970.
[20] *SMART* (V5.051) and *SAINT* (V5.00), Area detector control and integration software, Bruker AXS Inc., Madison,WI 53719, USA, **1998**.
[21] G. M. Sheldrick, *SHELXTL-97* (V5.10), Bruker AXS Inc., Madison, WI 53719, USA, **1997**.
[22] M. J. Frisch, G. W. Trucks, H. B. Schlegel, G. E. Scuseria, M. A. Robb, J. R. Cheeseman, V. G. Zakrzewski, J. A. Montgomery Jr, R. E. Stratmann, J. C. Burant, S. Dapprich, J. M. Millam, A. D. Daniels, K. N. Kudin, M. C. Strain, O. Farkas, J. Tomasi, V. Barone, M. Cossi, R. Cammi, B. Mennucci, C. Pomelli, C. Adamo, S. Clifford, J. Ochterski, G. A. Petersson, P. Y. Ayala, Q. Cui, K. Morokuma, D. K. Malick, A. D. Rabuck, K. Raghavachari, J. B. Foresman, J. Cioslowski, J. V. Ortiz, B. B. Stefanov, G. Liu, A. Liashenko, P. Piskorz, I. Komaromi, R. Gomperts, R. L. Martin, D. J. Fox, T. Keith, M. A. Al-Laham, C. Y. Peng, A. Nanayakkara, C. Gonzalez, M. Challacombe, P. M. W. Gill, B. G. Johnson, W. Chen, M. W. Wong, J. L. Andres, M. Head-Gordon, E. S. Replogle, J. A. Pople, *Gaussian 98*, revision A.7, Gaussian, Inc., Pittsburgh, PA, **1998**.
[23] U. Dörfler, D. L. Ormsby, R. Greatrex, J. D. Kennedy, *Inorg. Chim. Acta* **2000**, *304*, 268–273.

Received: March 14, 2007
Published Online: July 17, 2007

